AMERICAN SOCIETY FOR MICROBIOLOGY | Applied and Environmental Microbiology®

GENETICS AND MOLECULAR BIOLOGY

Analogous and Diverse Functions of APSES-Type Transcription Factors in the Morphogenesis of the Entomopathogenic Fungus *Metarhizium rileyi*

Caiyan Xin,[a] Jinping Zhang,[a] Siji Nian,[a] Guangxi Wang,[a] Zhongkang Wang,[b] Zhangyong Song,[a] Guangwei Ren[c]

[a]School of Basic Medical Sciences, Southwest Medical University, Luzhou, People's Republic of China
[b]Chongqing Engineering Research Center for Fungal Insecticide, School of Life Science, Chongqing University, Chongqing, People's Republic of China
[c]Institute of Qingdao Economic Crop Chinese Academy of Agricultural Sciences, Qingdao, People's Republic of China

Caiyan Xin and Jinping Zhang contributed equally to this work. Author order was determined by drawing straws.

ABSTRACT APSES-type transcription factors (TFs) have analogous and diverse functions in the regulation of fungal morphogenesis processes. However, little is known about these functions in microsclerotium formation. In this study, we characterized two orthologous APSES genes (*MrStuA* and *MrXbp*) in the entomopathogenic fungus *Metarhizium rileyi*. Deletion of either *MrStuA* or *MrXbp* impaired dimorphic transition, conidiation, fungal virulence, and microsclerotium formation. Compared with the wild-type strain, Δ*MrStuA* and Δ*MrXbp* mutants were hypersensitive to thermal and oxidative stress. Furthermore, transcriptome sequencing analysis revealed that MrStuA and MrXbp independently regulate their own distinctive subsets of signaling pathways during dimorphic transition and microsclerotium formation, but they also show an overlapping regulation of genes during these two distinct morphogenesis processes. These results provide a global insight into vital roles of MrStuA and MrXbp in *M. rileyi* and aid in dissection of the interacting regulatory mechanisms of dimorphism transition and microsclerotium development.

IMPORTANCE Transcription factors (TFs) are core components of the signaling pathway and play an important role in transcriptional regulation of gene expression during fungal morphogenesis processes. A prevailing theory suggests an interplay between different TFs regulating microsclerotial differentiation; however, the persisting issue remains that these interplay mechanisms are not clear. Here, we analyzed two members of the APSES-type TFs in *Metarhizium rileyi* using a gene deletion strategy and transcriptome analysis. Mutants were significantly impaired in microsclerotium formation and dimorphic transition. Transcriptome analysis provided evidence for interacting regulatory mechanisms by the two TFs in microsclerotium formation and dimorphic transition. Furthermore, we investigated their overlapping roles in mediating the expression of genes required for different fungal morphogenesis processes. Characterization of TFs in this study will aid in dissecting the interplay between regulatory mechanisms in fungal morphogenesis processes.

KEYWORDS *Metarhizium rileyi*, microsclerotium, morphogenesis, APSES-type transcriptional factors

Entomopathogenic fungi have been developed into many mycopesticides for the biological control of insect pests (1). *Metarhizium rileyi* (previously named *Nomuraea rileyi*) is a well-known dimorphic entomopathogenic fungus possessing a special dimorphic lifestyle with yeast-like hyphal bodies (referred to as yeast-like cells here) and a true filamentous growth phase *in vivo* and *in vitro* (2). Both the production of conidia, generally responsible for initiating infection on the cuticle of insect pests, and the

Citation Xin C, Zhang J, Nian S, Wang G, Wang Z, Song Z, Ren G. 2020. Analogous and diverse functions of APSES-type transcription factors in the morphogenesis of the entomopathogenic fungus *Metarhizium rileyi*. Appl Environ Microbiol 86:e02928-19. https://doi.org/10.1128/AEM.02928-19.

Editor Ning-Yi Zhou, Shanghai Jiao Tong University

Address correspondence to Zhangyong Song, szy83529@163.com.

Received 15 December 2019
Accepted 26 January 2020
Accepted manuscript posted online 31 January 2020
Published 1 April 2020

development of microsclerotium, an alternative fungal propagule for mycoinsectide, involve several morphological processes in *M. rileyi* (3, 4). Fungal morphogenesis is quite flexible in its adaptation to highly divergent metabolic and environmental changes (5, 6). A complex of signaling pathways has been confirmed, involving several transcription factors (TFs), each one acting singly or in combination to execute morphogenesis (7, 8). APSES-type TFs are fungal TFs with conserved basic helix-loop-helix (bHLH) DNA-binding domains, and the first members described were Asm1p in *Neurospora crassa*, Phd1p in *Saccharomyces cerevisiae*, Sok2p in *S. cerevisiae*, Efg1p in *Candida albicans*, and StuAp in *Aspergillus nidulans* (9–13), which are involved in the regulation of morphogenesis processes in fungi (14–17).

A similar set of APSES-type TFs exists in yeast and filamentous fungi, which have diverse functions. Phd1p is an activator, while Sok2p is a repressor regulating pseudohyphal growth in *S. cerevisiae* (18). Efg1p has dual role, whereas its homolog Efh1p is an activator in the regulation of morphogenesis and metabolism in *C. albicans* (19). Answi4, an APSES-type TF, plays only a weak role in the regulation of conidial color in *Aspergillus nidulans*; however, StuA regulates multicellular complexity during asexual reproduction (10, 11, 20). Investigations also found that the StuA homolog Mstu1 is indispensable for pathogenicity and that MoSwi6, another APSES-type TF, is required for pathogenicity in *Magnaporthe oryzae* (21, 22). Moreover, Mstu1 and MoSwi6 share a combining domain (22). These findings suggest that APSES members have analogous biological functions. However, the analogous and diverse roles of APSES-type TFs remain poorly understood in fungi.

Previous investigation revealed that deletion mutants of *MrSwi6*, an APSES-type TF gene in *M. rileyi*, show delayed dimorphic transition and reduced conidium and microsclerotium formation (23). Further comparative transcriptome analysis found that the *StuA* homolog *MrStuA* was upregulated and that another APSES-type DNA-binding domain gene (named *MrXbp*) was downregulated during *M. rileyi* microsclerotium formation (24). These results implied possible analogous and diverse functions of APSES-type TFs in the regulation of microsclerotium development. However, these functions have not been studied clearly.

Here, we investigated the functions of two APSES-type TFs (products of *MrStuA* and *MrXbp*) by constructing mutants for analyses of their multiple phenotypes. Different degrees of phenotypic changes highlighted their analogous and diverse roles in regulating dimorphic transition, conidial germination, multistress tolerance, fungal virulence, and conidium and microsclerotium development in *M. rileyi*. Furthermore, we probed the transcriptional network by which these two APSES-type TFs regulate dimorphic transition and microsclerotium development in *M. rileyi*.

RESULTS

Bioinformatic analysis. Orthologs of *MrStuA* and *MrXbp* (GenBank accession no. MN180231 and MN180232, respectively) were cloned from a previously prepared comparative transcriptome library (24). Genomic DNA sequences of *MrStuA* and *MrXbp* contained 2,113 bp and 1,570 bp and had 2 and 3 introns, respectively. Both MrStuA and MrXbp shared a conserved APSES-type DNA-binding domain. Additionally, MrStuA had a PAP1 superfamily domain (see Fig. S1A in the supplemental material). The deduced amino acid sequence of MrStuA presented similarities with those of APSES TFs of *Metarhizium guizhouense* (91% identity) (25) and *Metarhizium brunneum* (91% identity) (26). The deduced amino acid sequence of MrXbp showed similarities to those of the APSES-type DNA-binding domain protein of *Metarhizium robertsii* (57.8% identity) (26) and the transcription regulator HTH (55.8% identity) of *Metarhizium guizhouense* (25). In the phylogeny reconstruction, the protein sequences of MrStuA and MrXbp clustered together with those of other *Metarhizium* species (Fig. S1B).

To characterize the physiological functions of *MrStuA* and *MrXbp* in *M. rileyi*, gene deletion mutants (Δ*MrStuA* and Δ*MrXbp*) and corresponding complementation strains (Δ*MrStuA*+StuA and Δ*MrXbp*+Xbp) were generated, as described in the Materials and

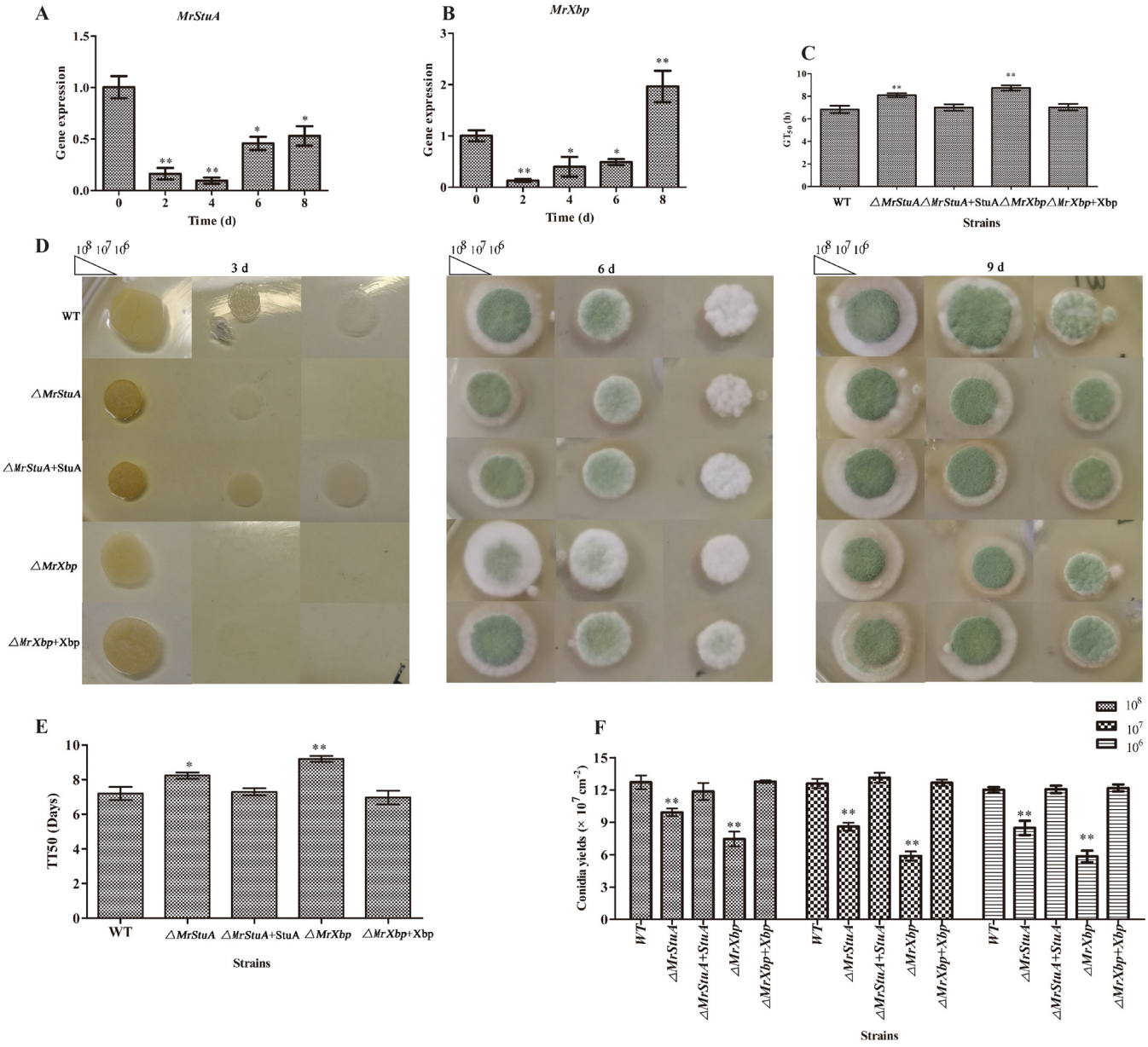

FIG 1 Function of MrStuA and MrXbp in conidium development. Transcription of *MrStuA* (A) and *MrXbp* (B) during conidiation. Conidial suspensions (2.5 μl; 10^7 conidia ml^{-1}) of the WT strain were spotted onto SMAY plates under continuous light at 25°C for 8 days. (C) GT_{50} as an index for conidial germination rate. (D) Images of various conidial suspensions spotted onto SMAY plates. (E) TT_{50} for transition of yeast-like cells to hyphae. TT_{50} was estimated using a Probit analysis with the SPSS software. (F) Statistical analysis of conidial yield. Error bars represent standard error. *, $P < 0.05$; **, $P < 0.01$; compared with wild-type strain.

Methods. All recombinant strains were verified by PCR and quantitative real-time PCR (RT-qPCR) screening (27) (see Fig. S2 in the supplemental material).

Roles of *MrStuA* and *MrXbp* in conidial development. *M. rileyi* CQNr01 (wild type [WT]) was grown on solid Sabouraud maltose agar fortified with 1% yeast extract (SMAY). Compared with expression levels at culture initiation (day 0), the expression of *MrStuA* and *MrXbp* was downregulated at the yeast-like cell period (day 2), hyphal period (day 4), and conidiation initiation (day 6) (Fig. 1A and B). Expression of *MrStuA* was downregulated (Fig. 1A), but expression of *MrXbp* was upregulated at the start of conidium maturation (day 8) (Fig. 1B). These results suggested that *MrStuA* and *MrXbp* may have analogous roles in the dimorphic transition and diverse roles in conidium maturation.

We assessed the median germination time (GT_{50}) for strains to reach 50% germination when incubated on SMAY at 25°C. Compared with the WT, the Δ*MrStuA* and Δ*MrXbp* mutants displayed defects in conidial germination (Fig. 1C) ($P < 0.01$). The GT_{50} of the Δ*MrStuA* mutant was 8.1 ± 0.3 h, whereas that of the WT was 6.8 ± 0.5 h, and that of the complementation strain was 7.0 ± 0.5 h ($P < 0.01$). The GT_{50} of the Δ*MrXbp* mutant was 8.7 ± 0.3 h and that of the complementation strain was 7.1 ± 0.4 h (Fig. 1C).

Further incubation on SMAY revealed that the dimorphic transition (day 3) was delayed in the Δ*MrStuA* and Δ*MrXbp* mutants, especially in suspensions at 10^6 conidia ml^{-1} (Fig. 1D). To further analyze the effect of MrStuA and MrXbp on dimorphic transition, we grew single yeast cells of WT and mutant strains on SMAY medium. These investigations showed that the median transition time required for 50% transition of yeast-like cells to hyphae (TT_{50}) in the Δ*MrStuA* mutant was 8.1 ± 0.3 days, that in the WT was 7.3 ± 0.1 days, and that in the complementation strain was 7.0 ± 0.1 days ($P < 0.05$) (Fig. 1E). The TT_{50} of the Δ*MrXbp* mutant was 9.2 ± 0.3 days and that of the complementation strain was 7.1 ± 0.3 days ($P < 0.001$) (Fig. 1E). These finding suggested that deletion of either *MrStuA* or *MrXbp* delays dimorphic transition. After 12 days, conidial yield of Δ*MrStuA* and Δ*MrXbp* mutants was 26% to 40% lower than that of WT and complemented strains (Fig. 1F). These results suggested that MrStuA and MrXbp have an important role in the regulation of dimorphic transition and conidium production.

Roles of *MrStuA* and *MrXbp* in activating signaling pathways during dimorphic transition. To identify the genes, signaling pathways, and metabolic pathways affected by *MrStuA* and *MrXbp* during dimorphic transition, we performed transcriptome sequencing analysis of the WT and Δ*MrStuA* and Δ*MrXbp* mutants. Results showed that 463 genes were upregulated and 201 genes were downregulated in the Δ*MrStuA* mutants, whereas 573 genes were upregulated and 1,127 genes were downregulated in the Δ*MrXbp* mutants compared with the WT (Fig. 2A). Among these differentially expressed genes (DEGs), 284 genes were regulated only by *MrStuA* and 1,320 genes were regulated only by *MrXbp* during dimorphic transition. Moreover, 380 genes were coregulated by *MrStuA* and *MrXbp* during dimorphic transition (Fig. 2B).

DEGs were functionally grouped into gene ontology (GO) classes comprising 37 functional categories in the Δ*MrStuA* mutants and 38 functional categories in the Δ*MrXbp* mutants (see Fig. S3 in the supplemental material). Moreover, we found 20 clusters of orthologous groups (COGs) in the Δ*MrStuA* mutants and 20 COGs in the Δ*MrXbp* mutants (see Fig. S4 in the supplemental material). A total of 91 DEGs in the Δ*MrStuA* mutants were assigned to 20 Kyoto Encyclopedia of Genes and Genomes (KEGG) enrichment pathways. The top three pathways were carbon metabolism (15.3%), biosynthesis of amino acids (14.2%), and oxidative phosphorylation (10.9%) (see Fig. S5A in the supplemental material). In contrast, a total of 279 DEGs in the Δ*MrXbp* mutants were assigned to 20 KEGG enrichment pathways. The top three pathways were ribosome (24.7%), biosynthesis of antibiotics (16.8%), and carbon metabolism (8.6%) (Fig. S5B).

To further investigate the mechanism of dimorphic transition regulated by *MrStuA* and *MrXbp*, we selected genes potentially involved in the dimorphic transition from transcriptome libraries (24) and examined these using transcriptional analysis. The following genes were selected: antioxidant enzyme genes (*MrCat1* for catalase-1 and *MrCat2* for catalase-2, *MrSod1* for superoxide dismutase-1, and *MrSod2* for superoxide dismutase-2), a determinant TF in response to oxidative stress (*MrAp1* for activator protein-1), pigment biosynthesis-related genes (*MrPks* for polyketide synthase and *MrLac* for laccase), mitogen-activated protein kinase (MAPK)-related genes (*MrSlt2* for Slt2-type MAPK, *MrHog1* for a stress-activated MAPK, and *MrSwi6* for an APSES-type TF), and cAMP signal transduction pathway-related genes (*MrPka* for the catalytic subunit of protein kinase A and *MrSok1* for cAMP-mediated signaling protein). Compared with the WT, the *MrAp1*, *MrPka*, *MrLac*, *MrHog1*, and *MrSok1* genes were upregulated in the Δ*MrStuA* mutants, whereas the *MrCat2* gene was downregulated (Fig. 2C). The *MrCat2*,

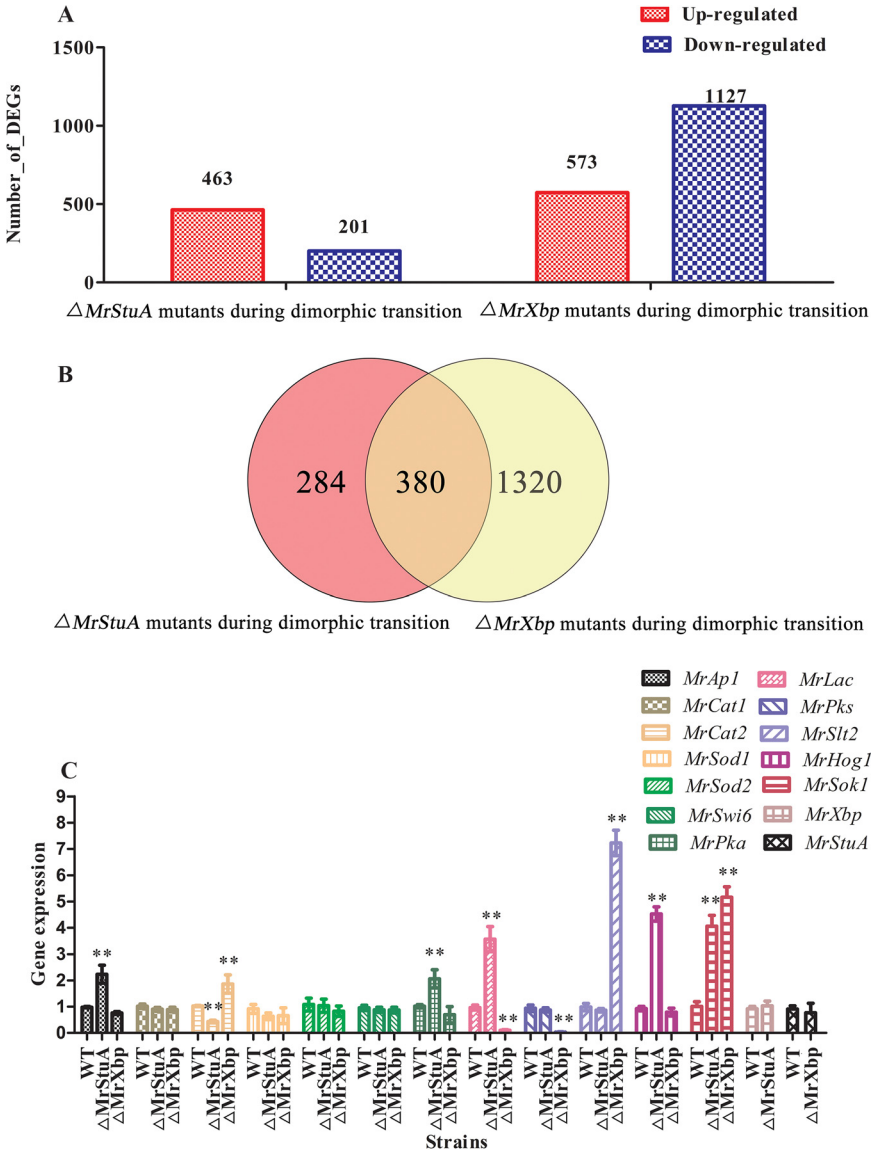

FIG 2 Comparative transcriptomic and RT-qPCR analysis of genes related to dimorphic transition. (A) DEGs in WT versus Δ*MrStuA* mutants and WT versus Δ*MrXbp* mutants during dimorphic transition. (B) Venn diagram showing the number of shared DEGs between WT versus Δ*MrStuA* mutants and WT versus Δ*MrXbp* mutants during dimorphic transition. (C) RT-qPCR analysis of genes. Error bars represent standard error. *, $P < 0.05$; **, $P < 0.01$; compared with wild-type strain.

MrSlt2, and *MrSok1* genes were upregulated in the Δ*MrXbp* mutants, whereas the *MrLac* and *MrPks* genes were downregulated compared with the WT (Fig. 2C).

Roles of *MrStuA* and *MrXbp* in microsclerotium development. To examine the function of MrStuA and MrXbp in microsclerotium development, we investigated the relative transcriptional levels of *MrStuA* and *MrXbp*. Results showed that the expression of *MrStuA* was downregulated during microsclerotium development (60 to 144 h) compared with that at the germinating spore stage (36 h) (Fig. 3A). However, the expression of *MrXbp* was downregulated during hyphal vegetative growth (60 h) and the microsclerotium initiation and formation periods (72 h and 96 h) but was upregulated during microsclerotium maturation (Fig. 3B). These results indicated that MrStuA and MrXbp may have analogous roles in the early stage of microsclerotium development and diverse roles in microsclerotium maturation.

After 72 h of incubation in liquid amended medium (AM) (4), WT and complemented strains started to form microsclerotium, whereas minimal vegetative growth was

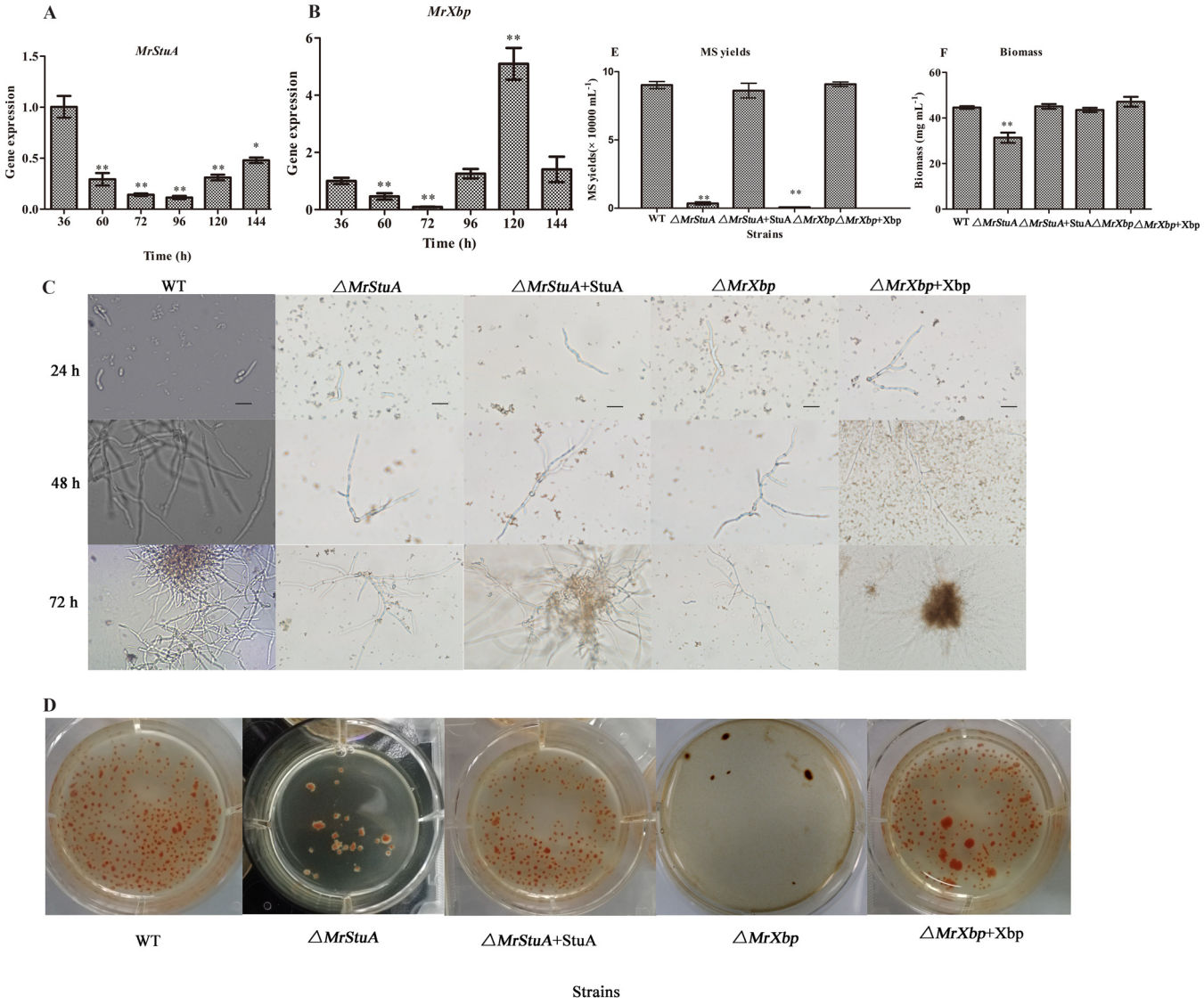

FIG 3 Gene expression and phenotypic characterization of microsclerotium development in AM. Transcription of *MrStuA* (A) and *MrXbp* (B) during microsclerotium development. (C) Development of microsclerotium in AM. Scale bars: 50 μm. (D) Phenotypic characterization of microsclerotium formation. Conidial suspensions were inoculated in AM and cultured for 6 days. (E) Microsclerotium yield and (F) biomass of the tested strains. Error bars represent standard error. *, $P < 0.05$; **, $P < 0.01$; compared with WT or results at 36 h.

observed in the Δ*MrStuA* and Δ*MrXbp* mutants (Fig. 3C). After incubation for 144 h, microsclerotium produced by WT strains matured and was accompanied by secondary mycelial growth, whereas the density of induced microsclerotium in the Δ*MrStuA* and Δ*MrXbp* mutants was significantly decreased (Fig. 3D) ($P < 0.001$). Microsclerotium yield of the Δ*MrStuA* mutants was reduced by approximately 95% compared with that of the WT (Fig. 3E), and biomass was decreased by 30% (Fig. 3F). Microsclerotium yield of the Δ*MrXbp* mutants was reduced by approximately 99% compared with that of the WT (Fig. 3E); however, there was no significant difference in biomass (Fig. 3F). Altogether, these results indicated that MrStuA and MrXbp play important roles in microsclerotium development.

Roles of *MrStuA* and *MrXbp* in activating signaling pathways during microsclerotium development. To identify the genes, signaling pathways, and metabolic pathways affected by MrStuA and MrXbp during microsclerotium development, we performed transcriptome sequencing analysis of WT and Δ*MrStuA* and Δ*MrXbp* mutants. Results showed that 465 genes were upregulated and 252 genes were downregulated

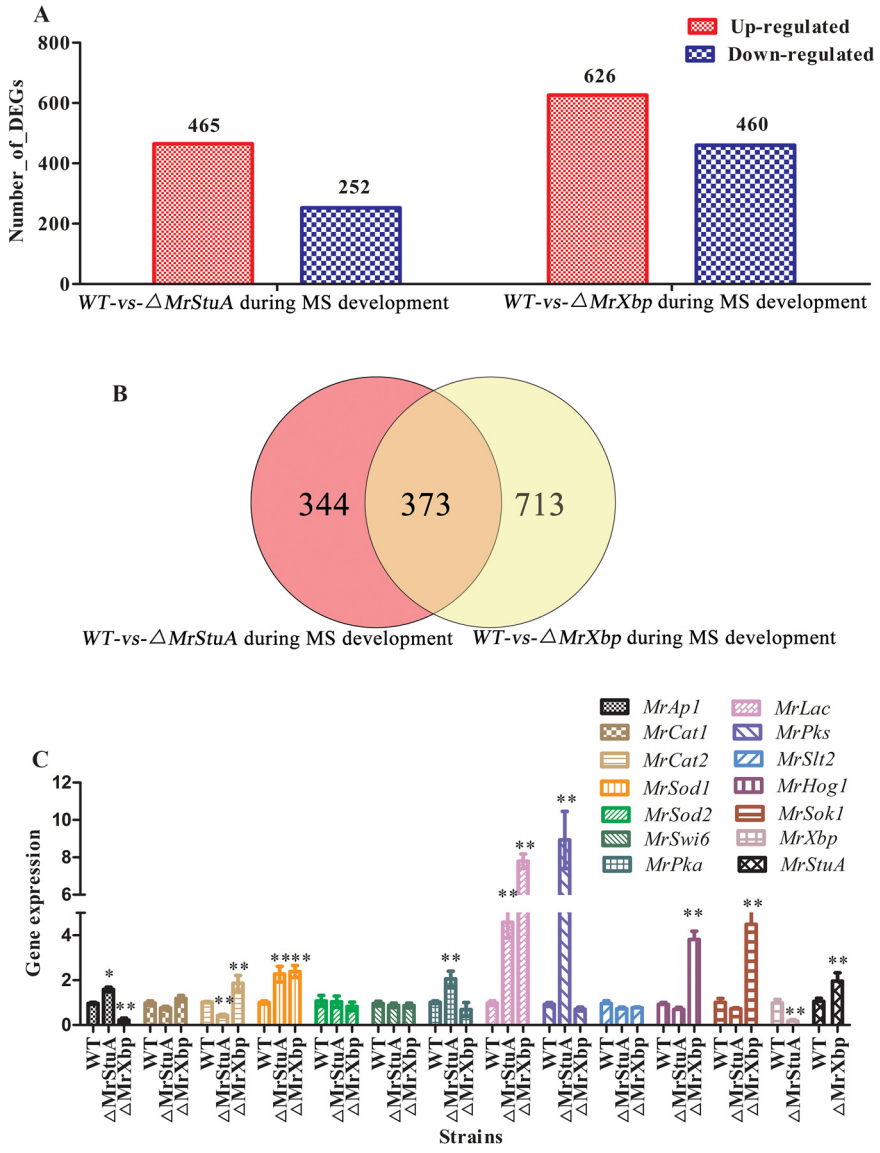

FIG 4 Comparative transcriptomic and RT-qPCR analysis of genes related to microsclerotium (MS) development. (A) DEGs in WT versus Δ*MrStuA* mutants and WT versus Δ*MrXbp* mutants during microsclerotium development. (B) Venn diagram showing the number of shared DEGs between WT versus Δ*MrStuA* mutants and WT versus Δ*MrXbp* mutants during microsclerotium development. (C) RT-qPCR analysis of genes. Error bars represent standard error. *, $P < 0.05$; **, $P < 0.01$; compared with wild-type strain.

in the Δ*MrStuA* mutants, whereas 626 genes were upregulated and 460 genes were downregulated in the Δ*MrXbp* mutants compared with the WT (Fig. 4A). Among these DEGs, 344 DEGs were regulated only by *MrStuA* and 713 DEGs were regulated only by *MrXbp* during microsclerotium development. Moreover, there were 373 DEGs coregulated by *MrStuA* and *MrXbp* during microsclerotium development (Fig. 4B).

DEGs were functionally grouped into GO classes representing 38 functional categories in the Δ*MrStuA* mutants and 40 functional categories in the Δ*MrXbp* mutants (see Fig. S6 in the supplemental material). Moreover, we found 20 COGs in the Δ*MrStuA* mutants and 21 COGs in the Δ*MrXbp* mutants (see Fig. S7 in the supplemental material). A total of 99 DEGs were assigned to 20 KEGG enrichment pathways in the Δ*MrStuA* mutants. The top three pathways were ribosome (21.2%), biosynthesis of amino acids (13.1%), and oxidative phosphorylation (9.1%) (see Fig. S8A in the supplemental material). A total of 129 DEGs were assigned to 20 KEGG enrichment pathways in the

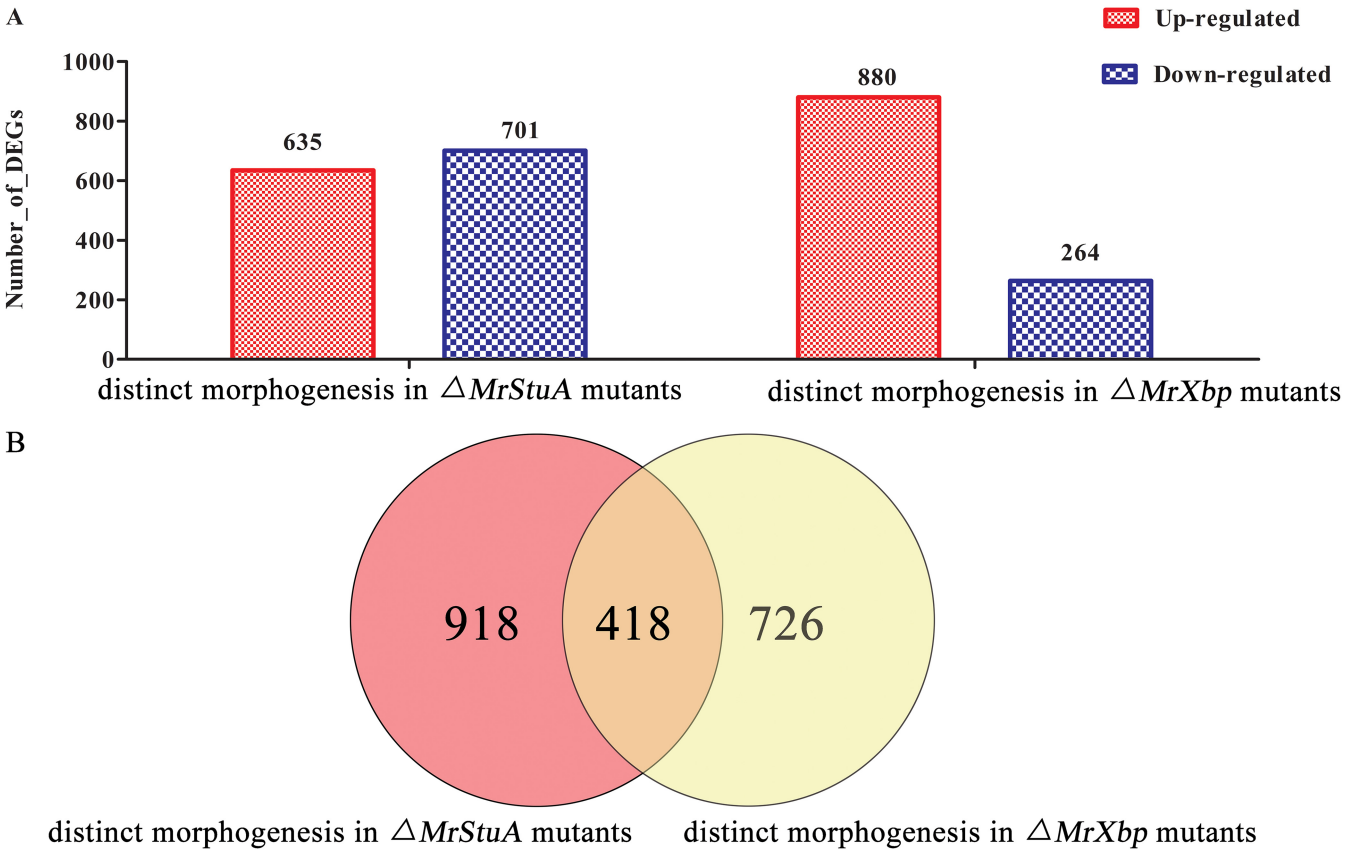

FIG 5 Overview of comparative transcriptomic data for the two morphogenesis processes. (A) DEGs of dimorphic transition versus microsclerotium development in Δ*MrStuA* mutants and Δ*MrXbp* mutants. (B) Venn diagram showing the number of shared DEGs between dimorphic transition and microsclerotium development in Δ*MrStuA* mutants and Δ*MrXbp* mutants.

Δ*MrXbp* mutants. The top three pathways were oxidative phosphorylation (11.6%), ribosome (11.6%), and tyrosine metabolism (7.8%) (Fig. S8B).

To further investigate the genes regulated by *MrStuA* and *MrXbp* during microsclerotium development, several groups of genes were analyzed by RT-qPCR. Compared with the WT, the *MrAp1*, *MrSod1*, *MrPka*, *MrLac*, and *MrPks* genes were upregulated, whereas *MrCat2* and *MrXbp* genes were downregulated in the Δ*MrStuA* mutants (Fig. 4C). The *MrCat2*, *MrSod1*, *MrHog1*, *MrSok1*, and *MrStuA* genes were upregulated, whereas the *MrAp1* gene was downregulated compared with the WT in the Δ*MrXbp* mutants (Fig. 4C).

Overview of comparative transcriptomic data. To confirm gene expression patterns obtained from transcriptome data, 14 genes from four sets of independent transcriptome data were analyzed by RT-qPCR (see Tables S1 to S4 in the supplemental material). Results showed that the transcriptome data and RT-qPCR were highly correlated (see Fig. S9 in the supplemental material).

Furthermore, we established an overview of DEGs associated with the two distinct morphogenesis processes (dimorphic transition versus microsclerotium development) in Δ*MrStuA* and Δ*MrXbp* mutants. In relation to their expression levels during dimorphic transition, 635 genes were upregulated and 701 genes were downregulated during microsclerotium development in Δ*MrStuA* mutants, whereas 880 genes were upregulated and 264 genes were downregulated during microsclerotium development in Δ*MrXbp* mutants (Fig. 5A). Among these DEGs, 918 DEGs were only regulated by *MrStuA* and 726 DEGs were only regulated by *MrXbp* in the two distinct morphogenesis processes. Moreover, there were 418 DEGs coregulated by *MrStuA* and *MrXbp* in the two processes (Fig. 5B).

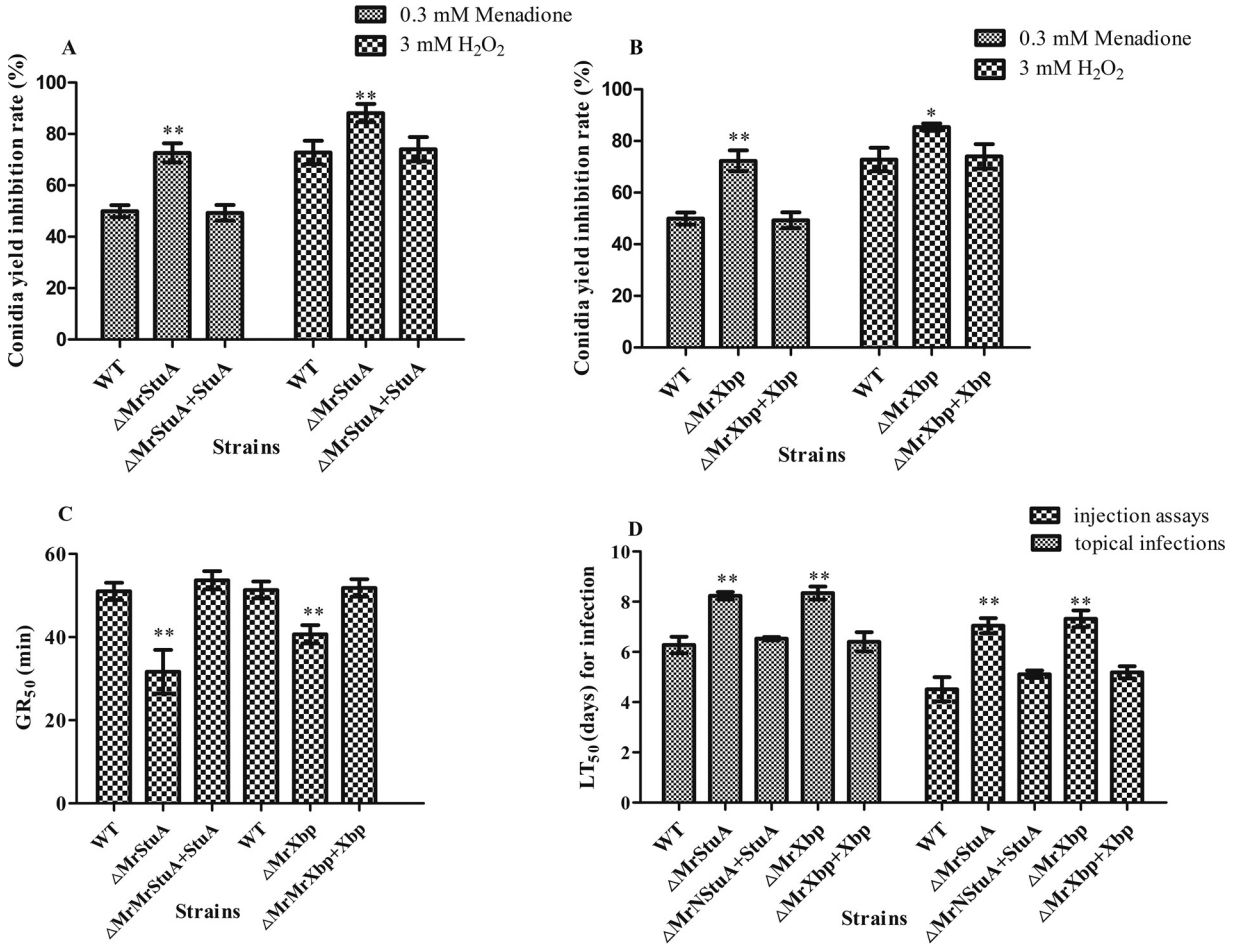

FIG 6 Deletion of *MrStuA* or *MrXbp* altered cellular sensitivity to oxidative stress, heat stress, and virulence. Statistical analysis of conidial yield inhibition rates under oxidative stress in (A) Δ*MrStuA* mutants and (B) Δ*MrXbp* mutants. (C) GR_{50} for conidial tolerance to heat stress at 45°C. (D) LT_{50} for the virulence of each strain. Data were estimated using a Probit analysis with the SPSS software. Error bars represent standard error. *, $P < 0.05$; **, $P < 0.01$; compared with WT.

DEGs associated with the two distinct morphogenesis processes were functionally grouped into GO classes representing 39 functional categories in Δ*MrStuA* mutants and 36 functional categories in Δ*MrXbp* mutants (see Fig. S10 in the supplemental material). We found 21 COGs in the Δ*MrStuA* mutants and 20 COGs in the Δ*MrXbp* mutants (see Fig. S11 in the supplemental material). A total of 209 DEGs were assigned to 20 KEGG enrichment pathways in the Δ*MrStuA* mutants (see Fig. S12A in the supplemental material). The top three pathways were biosynthesis of antibiotics (19.6%), carbon metabolism (11.0%), and biosynthesis of amino acids (9.5%). A total of 181 DEGs were assigned to 20 KEGG enrichment pathways in the Δ*MrXbp* mutants (Fig. S12B). The top three pathways were biosynthesis of antibiotics (18.2%), carbon metabolism (9.3%), and biosynthesis of amino acids (9.3%).

Roles of *MrStuA* and *MrXbp* in stress tolerance and virulence. Compared to the WT strain, *MrStuA* and *MrXbp* deletion mutants were significantly more sensitive to oxidative stress. Rates of conidial yield inhibition were increased by 17.2% to 45.3% ($P < 0.01$) in Δ*MrStuA* mutants and by 14.5% to 44.1% ($P < 0.05$) in Δ*MrXbp* mutants, compared with those of WT and complementation strains, respectively (Fig. 6A and B). These results indicate that *MrStuA* and *MrXbp* contribute to tolerance of oxidative stress.

Conidial thermotolerance was quantified as the germination rate resulting in 50% germination (GR_{50}) after exposure of conidial suspension to 45°C, as described previ-

ously (4). Compared with the WT strain, the GR_{50} for conidial tolerance to 45°C was shortened by 20.26% in the Δ*MrStuA* mutants (GR_{50}, 40.3 ± 3.7 min) and by 37.9% in the Δ*MrXbp* mutants (GR_{50}, 33.6 ± 4.4 min) (Fig. 6C). These results showed that MrStuA and MrXbp have analogous roles in response to thermal stress.

The mean lethal time (LT_{50}) of WT strains to kill 50% of *Spodoptera litura* larvae was 6.2 ± 0.4 days in topical bioassays for normal cuticle infection and 4.3 ± 0.5 days following injection for cuticle-bypassing infection bioassays (Fig. 6D). Compared with data from WT and complemented strains, lethal action through normal infection was delayed by 1.96 days in the Δ*MrStuA* mutants and 2.07 days in the Δ*MrXbp* mutants. The delay of lethal action following cuticle-bypassing infection increased to 2.75 days in the Δ*MrStuA* mutants and 3.02 days in the Δ*MrXbp* mutants (Fig. 6D). These results showed that lethal action was significantly delayed in the two mutants.

DISCUSSION

Developmental processes play important roles in the life cycle of ascomycete fungi. Here, we systematically characterized *MrStuA* and *MrXbp*, encoding two members of the APSES-type TFs that have essential roles in dimorphic transition, thermotolerance, oxidative adaptation, conidium and microsclerotium development, and virulence. We additionally identified commonalities and differences in the regulation of gene expression during the developmental processes of dimorphic transition and microsclerotium formation.

The conidiation process in filamentous fungi is a precisely timed and genetically programmed event that occurs from vegetative growth to asexual development (28). Although signaling pathways regulating dimorphic transition and conidiation in *Metarhizium* species are well characterized (23, 27, 29–32), no member of the APSES family has been characterized in entomopathogenic fungi. Similar to Asm1p in *N. crassa* (9), StuA in *A. nidulans* (11), FgStuA in *Fusarium graminearum* (33), and Vst1 in *Verticillium* species (16), mutation of *MrStuA* appeared to interfere with conidiation (Fig. 1). Previous investigations also identified diverse functions of the APSES TFs in different fungal species. For instance, chlamydospore formation is dramatically promoted in *Fusarium oxysporum* Δ*FoStuA* mutants, but these phenotypes are not observed in *F. graminearum* Δ*FgStuA* mutants (33). Unlike the highly conserved DNA-binding motif of MrStuA, MrXbp homologs show low similarity among different species. Furthermore, to our knowledge, no studies on the biological functions of Xbp in fungi have been reported. Interestingly, a decrease conidial yield in Δ*MrXbp* mutants was observed (Fig. 1).

Meanwhile, similar to the Δ*MrSwi6* mutants (23) and Δ*MrStuA* mutants in *M. rileyi*, we also observed a delay in dimorphic transition in the Δ*MrXbp* mutants (Fig. 1). Dimorphic transition is critical for pathogenesis, virulence, and the life cycle of dimorphic fungi (2, 4). Recent investigations confirmed that many signaling pathways, including activator protein-1 (29), cell wall integrity (23, 34), and high osmolarity glycerol (27) signaling pathways, take part in the regulation of morphology. Furthermore, various conidial suspensions of strains had different dimorphic transition rates, demonstrating again that there is quorum sensing in the dimorphic transition of *M. rileyi* (23). However, the molecular mechanism of quorum sensing is complex (35). To investigate the mechanisms of dimorphic transition regulated by APSES TFs, we conducted comparative transcriptomic analysis. Results revealed not only analogous but also distinct strategies in the regulation of dimorphic transition by the two APSES-type TFs in *M. rileyi* (Fig. 2). *StuA* homologs in fungi are targets of the cAMP/protein kinase A (PKA) signal transduction pathway (10, 16, 36, 37). The expression of cAMP signal transduction pathway-associated genes was significantly changed during dimorphic transition in Δ*MrStuA* mutants, adding further evidence to support this viewpoint. The oxidative stress triggers dimorphic transition in *M. rileyi* (27). The *MrAp1* gene was significantly upregulated in Δ*MrStuA* mutants, indicating overlapping between MrStuA and MrAp1 with the PAP1 domain during dimorphic transition. Moreover, no significant change among the three APSES-type TFs (MrSwi6, MrStuA, and MrXbp) and different signaling pathways

with different expression patterns were found in *MrStuA* and *MrXbp* single-deletion mutants during dimorphic transition (Fig. 2C).

Melanized microsclerotium formation induced in liquid culture is also a complex development process (8). Similar to Vst1 in *Verticillium* species (16), the APSES TFs are key regulators of microsclerotium development (Fig. 3). Our previous study demonstrated that intracellular oxidative stress can trigger microsclerotium differentiation (24, 27) and that MrAp1 plays an important role in mediating redox homeostasis during microsclerotium development (27). Our analysis found that expression of *MrAp1* was upregulated in Δ*MrStuA* mutants; however, it was downregulated in Δ*MrXbp* mutants (Fig. 4C), indicating that the two fungal TFs have diverse regulatory patterns in their interactions with *MrAp1* during microsclerotium development. Further investigations confirmed 57 genes coregulated by the three TFs during *M. rileyi* development (see Fig. S13 in the supplemental material). Moreover, investigations revealed downregulated expression of *MrXbp* following a single deletion of *MrStuA* and upregulated expression of *MrStuA* following a single deletion of *MrXbp*, indicating that these two APSES TF genes have overlapping regulatory patterns during microsclerotium development (Fig. 4C). Transcriptomic analysis identified oxidative phosphorylation as the major analogous KEGG enrichment pathway (Fig. S8).

Specialized cellular differentiation of fungal growth under different conditions requires spatial and temporal regulation of gene expression. Unlike MrStuA, which plays opposite roles to cAMP/PKA and AP-1 signaling pathways during dimorphic transition and microsclerotium development, MrXbp has varied regulatory patterns on the growth of *M. rileyi* in liquid and solid conditions but has overlapping regulatory patterns with MrStuA (Fig. 2, 4, and 5). Transcriptomic analysis identified 13 identical and 7 distinctive KEGG enrichment pathways regulated by the two APSES-type TFs during dimorphic transition and microsclerotium formation (Fig. S12). However, simultaneous knockout of *MrStuA* and *MrXbp* has not been successful despite many attempts. Further experiments are needed to elucidate the details of the varied regulatory patterns by the two APSES-type TFs.

Successful insect infection by entomopathogenic fungi is highly related to appressorium formation, morphological form shifting, utilization of nutrition from the host, and adaptation to stress from the host (30, 32). Similar to observations in *Leptosphaeria maculans* (37) and *Stagonospora nodorum* (38) and unlike those in *Verticillium* species (16), deletion of *MrStuA* resulted in decreased virulence (Fig. 6). Moreover, virulence assays revealed that Δ*MrXbp* mutants were significantly less virulent than the WT strain. Possible explanations for this are reduced dimorphic transition and hypersensitivity to oxidative stress.

In the present study, we dissected the regulatory roles of *MrStuA* and *MrXbp* in dimorphic transition, conidium and microsclerotium development, and stress tolerance in the entomopathogenic fungus *M. rileyi*, providing innovative information on the regulatory mechanisms of fungal morphogenesis. Such systematic and transcriptome-wide characterization can be effectively used to generate more information on the regulatory mechanisms of fungal morphogenesis processes.

MATERIALS AND METHODS

Fungal strains and culture conditions. *M. rileyi* strain CQNr01 was obtained from the Engineering Research Center for Fungal Insecticides, Chongqing, China. All strains used in this study were cultured on SMAY for conidiation assays or in AM culture for microsclerotium assays, according to previous methods (29). *Escherichia coli* DH5α (Invitrogen, Shanghai, China) was used for recombinant DNA manipulation. *Agrobacterium tumefaciens* AGL-1 (Invitrogen) was used for fungal transformations. These bacteria were cultured according to previously described methods (29).

Bioinformatics and phylogenetic analysis. *MrStuA* and *MrXbp* genes were amplified using primers *MrStuA-F/MrStuA-R* and *MrXbp-F/MrXbp-R* based on sequences of a previously published transcriptome library (24) (Table 1). Protein sequences were aligned using InterProScan (http://www.ebi.ac.uk/Tools/pfa/iprscan) and DNAMAN software (Lynnon Corporation). Phylogenetic trees were generated using MEGA 6.0 (39).

Construction of deletion and complementation mutants. The 5′ and 3′ flanking sequences of *MrStuA* and *MrXbp* genes were amplified from the *M. rileyi* genome database (NCBI accession no. AZHC00000000.1) (25) via PCR and inserted independently into Pzp-Ptrpc-Hph-Knock (resistance to

TABLE 1 Oligonucleotide primers used in this study

Usage	Primer	Sequence (5′ to 3′)
PCR of the genomic DNA sequences	*MrXbp-F*	CGACCCCTTCCAACTCAAACGCAC
	MrXbp-R	CTCCCACCCGTGCCACTTTTCCCC
	MrStuA-F	AAGACCCTCCTTCCGACCTCCTCT
	MrStuA-R	TATAACCCACAGCAAGTCGTCAAC
Used as construction of gene disruption vector	*MrXbp*LF	CGGAATCAGTCAGCCCTCTCGGGTCCGTCATC
	*MrXbp*LR	CCGCTCGAGCTGTGGGCAGATGCTTCGTGGTTCA
	*MrXbp*RF	GCTCTAGATGGAAGCGTTATCAGAGCAGAGCGA
	*MrXbp*RR	AACTGCAGGGCAAGTCACCACGAGCCCCGAGGG
	*MrSt*LF	CGGAATTCGGCATTTCAAGTGAACACCAAGTCTT
	*MrSt*LR	CCGCTCGAGATCATTTGGCAGATTGGACGACGGTA
	*MrSt*RF	GCTCTAGATATCTCGCCACACATCTTTCAAGCAA
	*MrSt*RR	CCCAAGCTTAGGCACAGGGTGGAATGTATCGGCTA
Used as construction of gene complementation plasmid	*MrXbp*-HF	CCGCTCGAGCTCGGGCAAGGGCAAAGGCTCACA
	MrXbp-HR	GCTCTAGACGATGCCTGGGTGAAGCGGTTCAAG
	MrSt-HF	GCTCTAGAGGAGTGTCCATCAATGTTCCGTAGT
	MrSt-HF	AACTGCAGAACAGGCGTGCTAAGTAACATAGAA
Mutants by PCR verification	*MrXbp*F	CTCGGGCAAGGGCAAAGGCTCACA
	*MrXbp*R	GCACCTCGCTGCCAATAATGAAGA
	MrXbp-OF	CCAGGCAGATAATAACAGCATTCA
	MrXbp-OR	TCGCTTTATTCGGATTCCTACTTC
	*MrSt*R	TTGGGCAGTCTGACGGTTCAAGCC
	*MrSt*F	TTGACCCAGAACTCTAAACCAGCA
	MrSt-OF	ATGGGAGGATGAAGGCAGTCTGTG
	MrSt-OR	CATTACCCATACCATTGGCTTCACT
	hph-F	GCTCTCGCTAAACTCCCCAATGTCA
	hph-R	CATTGACTGGAGCGAGGCGATGTTC
RT-qPCR analysis	*MrXbp-qF*	GCATTCAATGTCTCGCAGTT
	MrXbp-qR	ATTCGTGGGAATCTGAAAGG
	MrSt-qF	TCACTACGCTGGGTTCGATA
	MrSt-qR	TTCGACCTGAAAGCACAGAC
	Mrtef-qF	GTCATCGTCCTCAACCATC
	Mrtef-qR	CAGTCTCAACAGCCTTACC
	Mrtub-qF	GGCAAGGTCGCTATGAAG
	Mrtub-qR	CTGGATGGAGGTAGAGTTAC
	MrCat1-qF	GAGCCAGCCTCGTCTGTTCT
	MrCat1-qR	CTGGGCGAGGACGTTCTTCT
	MrCat2-qF	AAGGATCCGCAGAAGCGTGA
	MrCat2-qR	AAGGTGTGGCCTCCAGCAAT
	MrSod1-qF	TGCCTGCTTTATCAATCGAC
	MrSod1-qR	TCAAGAATGAGTGTGCGTCA
	MrSod2-qF	AGGTTCTCCCAGAAGAGGGA
	MrSod2-qR	CGTACGTGACGAACCTCAAC
	MrAp1-qF	ACATACGCCCAGAAAGAACC
	MrAp1-qR	AGTTGGTTGCAGCTCAAATG
	MrH101-qF	TGGAGAAGCGTTTGGAGGAT
	MrH101-qR	GCCACCAGAAGCATTGAGAG
	MrCp450-qF	CTATATGGCACGTCCACGAC
	MrCp450-qR	GCTACGATTCCTTGGTTGGT
	MrHog1-qF	GCATCGTGACTTGAAGCCTA
	MrHog1-qR	GGGCTCGGTAATATCGTGTT
	MrSlt2-qF	TGTGCGGCCTCAAGTATATC
	MrSlt2-qR	CGAGGCCAAAGTCACAGAT
	MrHapX-qF	AGCCACAGGAACTTCTCCAA
	MrHapX-qR	GACGCTCATGATGCTAGCTG
	MrPkac-qF	AGGAGGTTGGTGATGAAGGG
	MrPkac-qR	CCCAAGTATACGCGCTCAAG
	MrCwb-qF	GGTGATTTCTCGTGGCTGTC
	MrCwb-qR	GGCCTCTCGTCGAAATCTTG
	MrCel-qF	GAAATCTCGGCCACGTTCAA
	MrCel-qR	GGAGAGACTTGGACGCTGTA
	MrH90-qF	CCCAGAGACAAGCAACGAAG
	MrH90-qR	TCTCGCCCAAGTCTCTCATC

(Continued on next page)

TABLE 1 (Continued)

Usage	Primer	Sequence (5′ to 3′)
	MrPtp -qF	GCAGTTTCCGCTTCTCGATT
	MrPtp -qR	CTGTGATTGTCCAGCTCACG
	MrNsdD-qF	CAACGGAGCATATGGTCATC
	MrNsdD-qR	CATGCCTAGGTGAGACTGGA
	Mrlac-qF	AGTGCACCGCAAACAATCAT
	Mrlac-qR	GCGACTGTCTGGTTGAAGAC
	MrCcp-qF	GTCCTTGGTAGGGTTGACGA
	MrCcp-qR	ATGGTACTCTGAGCCTGCTG
	Mrpks-qF	GCCTCCTCCATCGTCAAGGT
	Mrpks-qR	GCGCTCGTCTCGAGGAAGTA
	MrAtp10-qF	TCTTCTGTCGGCTCTGGTTT
	MrAtp10-qR	AAGCTTCGAGTCTCCCACAA
	MrWsc-qF	CGGGCGATTTGACTCTTGTT
	MrWsc-qR	GTTGTGTTGTCGAAGGCAGT
	MrMas1-qF	ACGAACAATGCACACGTTCT
	MrMas1-qR	CTTCACTGGCTTGTCCATCG
	MrClp-qF	TCACTAGAACTTGCCTGCCA
	MrClp-qR	TTCTGGCTCTATGGCTACGG
	MrRad2-qF	CTGAGTGTCAGCGACTGTTG
	MrRad2-qR	TCCTTCCGCTGCTCACTAAA
	MrEmk1-qF	CGAGAATGTTGGAGGGCTTG
	MrEmk1-qR	TCGAGTGTCGAGGGTATTCG
	MrTapt1-qF	CGAGGTAGACCAGGACCATC
	MrTapt1-qR	TTCCATATCGTGCCTCGTGA
	MrMob-qF	CCTGACGTTACACCGTTGAC
	MrMob-qR	TAGGATGGTGCAGTTGAGCA
	MrSem-qF	GACTTGTTTCTCCCGGTTCG
	MrSem-qR	CTGACCAGCAACGAAGAAGG
	MrUce-qF	CGCTTCCCTACCGAATACC
	MrUce-qR	TCGTCGCCTGGTCTGTGGA
	MrSwi6-qF	CCACCCAGATTCTCAAGGTT
	MrSwi6-qR	TGCTCGCCTGTTTGTATCTC
	MrSok1-qF	GACCAACAACAACAGCCACT
	MrSok1-qR	TCTTGTCCGTCCCGTAACAA

hygromycin B). Disruption vectors were introduced into *M. rileyi* via *Agrobacterium* sp.-mediated transformation as described previously (29). Transformants were selected and gene mutants were verified by PCR using a combination of primers targeting flanking regions (*MrSt*F/*MrSt*R or *MrXbp*F/*MrXbp*R) (Table 1), primers annealing within introduced cassettes (*hph*-F/*hph*-R), and another pair of primers identifying the open reading frame (ORF) (*MrSt*-OF/*MrSt*-OR or *MrXbp*-OF/*MrXbp*-OR) (Table 1). PCR sequences were then sequenced. Complementation of Δ*MrStuA* mutants or of Δ*MrXbp* mutants was performed by introducing the complementation vector Pzp-Sur-cassette (resistance to sulfonylurea). ORFs of *MrStuA* and *MrXbp* with their promoter and terminator regions were amplified using primers *MrSt*-HF/*MrSt*-HR and *MrXbp*-HF/*MrXbp*-HR, respectively (Table 1). PCR products were digested by restriction endonucleases and inserted into the Pzp-Sur-cassette to generate complementation vectors (Pzp-Sur-MrStuA and Pzp-Sur-MrXbp). The vectors were introduced into gene mutants via *Agrobacterium* sp.-mediated transformation, and transformants were screened as described previously (29).

Phenotypic experiments. To investigate the role of MrStuA and MrXbp on dimorphic transition, vegetative growth, and conidial development, conidial suspensions (10^6, 10^7, and 10^8 conidia ml^{-1}) were pipetted onto SMAY plates under continuous light at 25°C for 12 days. After 6 days of incubation, three culture plugs (5 mm diameter) were removed every 3 days from each plate using a cork borer. The concentration of conidia was counted as described previously (29). Colony morphology was investigated, and images were collected using a digital camera (60-mm macro lens; Canon Inc., Tokyo, Japan).

To evaluate the influence of Δ*MrStuA* and Δ*MrXbp* mutants on dimorphic transition, switching rates of different strains were counted as described previously (27). Briefly, approximately 100 simple yeast cells were pipetted onto SMAY medium and regularly observed for colony morphology. Switching rates at various time points were recorded, and TT_{50} was estimated.

Conidial germination investigations were conducted as described previously (4). Briefly, conidial suspensions (1×10^7 conidia) were spread evenly onto SMAY plates and incubated at 25°C. After inoculation for 14 h, conidial germination rates were assessed every 2 h until full germination. Conidial thermotolerance was quantified as the germination rate resulting in 50% germination after exposure at 45°C for 0 to 120 min (4). Conidial oxidative stress tolerance was assessed after incubation on SMAY plates containing 0.03 mM menadione and 3 mM H_2O_2. Conidial suspensions (1×10^8 conidia) were pipetted and cultured at 25°C. Conidial yields were counted at 12 days postincubation. The conidium yield inhibition rate was calculated relative to untreated controls, where inhibition rate (%) = (number of untreated colonies – number of treated colonies)/number of untreated colonies × 100.

To evaluate the roles of *MrStuA* and *MrXbp* in microsclerotium development, conidial suspensions (1×10^7 conidia) were inoculated in AM culture for 6 days as described previously (4). Biomass and microsclerotium yield were quantified as described previously (4). Microsclerotium morphologies were observed using the digital camera and a microscope.

Transcriptional analysis. To determine time-specific expression patterns of *MrStuA* and *MrXbp* during microsclerotium development, samples of WT inoculated in AM were collected at 36 h (yeast-like cell period), 60 h (hyphal elongation and microsclerotium initiation period), 72 h (microsclerotium formation), 96 h (mass microsclerotium formation), and 120 h (microsclerotium maturation) for RNA extraction. To determine time-specific expression patterns during conidiation, samples of WT inoculated onto SMAY were collected at 0 days (the start of incubation), 2 days (yeast-like cells period), 4 days (hyphal period), 6 days (conidiation initiation), and 8 days (the start of conidium maturation) for RNA extraction. Gene expression patterns were confirmed for samples of each strain cultured in AM for 72 h or on SMAY for 3 days. Total RNA samples were collected using the RNAiso plus reagent (TaKaRa, Dalian, China) and reverse-transcribed into cDNA using PrimeScript RT master mix (TaKaRa). RT-qPCR was performed using SYBR green detection. Transcripts of β-tubulin (*Mrtub*) and translation elongation factor (*Mrtef*) genes were used as internal standards. Transcript ratios were evaluated using the $2^{-\Delta\Delta CT}$ method (40).

Digital gene expression profiling analysis. To further study the expression patterns of *MrStuA* and *MrXbp* prior to dimorphic transition and microsclerotium development, transcriptome sequencing analysis was performed. Total RNA extraction from three replicate samples, library construction, and sequencing were performed as described previously (29). Genes with fold change of $\geq$2 and false discovery rate (FDR) of $<$0.01 were considered significantly differentially expressed. DEGs were identified using DESeq software (41). DEGs were annotated and assigned functional categories using MapMan annotation (42).

Insect bioassays. Bioassays were conducted against third-instar larvae according to previously described methods (27). Briefly, topical infections were performed by immersing larvae in conidial suspensions (1×10^7 conidia). For injection assays, each insect was injected with the conidial suspension (1×10^6 conidia). Three replicate groups comprising 30 larvae each were tested. The mortality rate was recorded daily, and LT_{50} values were determined by Probit analysis with the SPSS program (SPSS Inc., Chicago, IL, USA).

Statistical analysis. All assays were repeated three times. Differences in the data were analyzed by one-way analysis of variance (ANOVA), and significance was determined by Duncan's multiple range tests using SPSS 17.0 software. Graphs were constructed with GraphPad Prism 5 software (GraphPad Software Inc., La Jolla, CA, USA). Error bars represent standard error.

Data availability. The mRNA raw sequence data were deposited in the Beijing Institute of Genomics Genome Sequence Archive (http://gsa.big.ac.cn/) with the accession number PRJCA002177 (https://bigd.big.ac.cn/search?dbId=bioproject&q=PRJCA002177+). Orthologs of *MrStuA* and *MrXbp* were deposited in GenBank under accession numbers MN180231 and MN180232, respectively.

SUPPLEMENTAL MATERIAL

Supplemental material is available online only.

SUPPLEMENTAL FILE 1, PDF file, 2.5 MB.

ACKNOWLEDGMENTS

This research was supported financially by the National Natural Science Foundation of the China (no. 31701127), Science and Technology Project of Sichuan (no. 2019YJ0407) and Luzhou (no. 2018-JYJ-32), and Major Special Projects (no.110201601023(LS-03)).

We declare that we have no conflict of interest.

REFERENCES

1. de Faria MR, Wraight SP. 2007. Mycoinsecticides and mycoacaricides: a comprehensive list with worldwide coverage and international classification of formulation types. Biol Control 43:237–256. https://doi.org/10.1016/j.biocontrol.2007.08.001.
2. Pendland JC, Boucias DG. 1997. *In vitro* growth of the entomopathogenic hyphomycete *Nomuraea rileyi*. Mycologia 89:66–71. https://doi.org/10.2307/3761173.
3. Fronza E, Specht A, Heinzen H, de Barros NM. 2017. *Metarhizium (Nomuraea) rileyi* as biological control agent. Biocontrol Sci Techn 27:1243–1264. https://doi.org/10.1080/09583157.2017.1391175.
4. Song ZY, Yin YP, Jiang SS, Liu JJ, Wang ZK. 2014. Optimization of culture medium for microsclerotia production by *Nomuraea rileyi* and analysis of their viability for use as a mycoinsecticide. BioControl 59:597–605. https://doi.org/10.1007/s10526-014-9589-4.
5. Gauthier GM. 2015. Dimorphism in fungal pathogens of mammals, plants, and insects. PLoS Pathog 11:e1004608. https://doi.org/10.1371/journal.ppat.1004608.
6. Wang LQ, Lin XR. 2012. Morphogenesis in fungal pathogenicity: shape, size, and surface. PLoS Pathog 8:e1003027. https://doi.org/10.1371/journal.ppat.1003027.
7. Shelest E. 2017. Transcription factors in fungi: TFome dynamics, three major families, and dual-specificity TFs. Front Genet 8:53. https://doi.org/10.3389/fgene.2017.00053.
8. Song ZY. 2018. Fungal microsclerotia development: essential prerequisite, influence factors, and molecular mechanism. Appl Microbiol Biotechnol 102:9873–9880. https://doi.org/10.1007/s00253-018-9400-z.
9. Aramayo R, Peleg Y, Addison R, Metzenberg R. 1996. Asm-1, a *Neurospora crassa* gene related to transcriptional regulators of fungal development. Genetics 144:991–1003.
10. Bockmühl DP, Ernst JF. 2001. A potential phosphorylation site for an

A-type kinase in the Efg1 regulator protein contributes to hyphal morphogenesis of *Candida albicans*. Genetics 157:1523–1530.
11. Miller KY, Wu J, Miller BL. 1992. StuA is required for cell pattern formation in *Aspergillus*. Genes Dev 6:1770–1782. https://doi.org/10.1101/gad.6.9.1770.
12. Gimeno CJ, Fink GR. 1994. Induction of pseudohyphal growth by overexpression of PHD1, a *Saccharomyces cerevisiae* gene related to transcriptional regulators of fungal development. Mol Cell Biol 14:2100–2112. https://doi.org/10.1128/mcb.14.3.2100.
13. Ward MP, Gimeno CJ, Fink GR, Garrett S. 1995. SOK2 may regulate cyclic AMP-dependent protein kinase-stimulated growth and pseudohyphal development by repressing transcription. Mol Cell Biol 15:6854–6863. https://doi.org/10.1128/mcb.15.12.6854.
14. Mancera E, Porman AM, Cuomo CA, Bennett RJ, Johnson AD. 2015. Finding a missing gene: *EFG1* regulates morphogenesis in *Candida tropicalis*. G3 (Bethesda) 5:849–856. https://doi.org/10.1534/g3.115.017566.
15. Ohara T, Tsuge T. 2004. FoSTUA, encoding a basic helix-loop-helix protein, differentially regulates development of three kinds of asexual spores, macroconidia, microconidia, and chlamydospores, in the fungal plant pathogen *Fusarium oxysporum*. Eukaryot Cell 3:1412–1422. https://doi.org/10.1128/EC.3.6.1412-1422.2004.
16. Sarmiento-Villamil JL, García-Pedrajas NE, Baeza-Montañez L, García-Pedrajas MD. 2018. The APSES transcription factor Vst1 is a key regulator of development in microsclerotium- and resting mycelium-producing *Verticillium* species. Mol Plant Pathol 19:59–76. https://doi.org/10.1111/mpp.12496.
17. Wang Q, Szaniszlo PJ. 2007. WdStuAp, an APSES transcription factor, is a regulator of yeast-hyphal transitions in *Wangiella (Exophiala) dermatitidis*. Eukaryot Cell 6:1595–1605. https://doi.org/10.1128/EC.00037-07.
18. Ramírez-Zavala B, Domínguez A. 2008. Evolution and phylogenetic relationships of APSES proteins from Hemiascomycetes. FEMS Yeast Res 8:511–519. https://doi.org/10.1111/j.1567-1364.2008.00370.x.
19. Doedt T, Krishnamurthy S, Bockmuhl DP, Tebarth B, Stempel C, Russell CL, Brown AJP, Ernst JF. 2004. APSES proteins regulate morphogenesis and metabolism in *Candida albicans*. Mol Biol Cell 15:3167–3180. https://doi.org/10.1091/mbc.e03-11-0782.
20. Lee J-Y, Kim L-H, Kim H-E, Park J-S, Han K-H, Han D-M. 2013. A putative APSES transcription factor is necessary for normal growth and development of *Aspergillus nidulans*. J Microbiol 51:800–806. https://doi.org/10.1007/s12275-013-3100-2.
21. Nishimura M, Fukada J, Moriwaki A, Fujikawa T, Ohashi M, Hibi T, Hayashi N. 2009. Mstu1, an APSEE transcription factor, is required for appressorium-mediated infection in *Magnaporthe grisea*. Biosci Biotechnol Biochem 73:1779–1786. https://doi.org/10.1271/bbb.90146.
22. Qi ZQ, Wang Q, Dou XY, Wang W, Zhao Q, Lv RL, Zhang HF, Zheng XB, Wang P, Zhang ZG. 2012. MoSwi6, an APSES family transcription factor, interacts with MoMps1 and is required for hyphal and conidial morphogenesis, appressorial function, and pathogenicity of *Magnaporthe oryzae*. Mol Plant Pathol 13:677–689. https://doi.org/10.1111/j.1364-3703.2011.00779.x.
23. Wang ZK, Yang J, Xin CY, Xing XR, Yin YP, Chen L, Song ZY. 2019. Regulation of conidiation, dimorphism transition, and microsclerotia formation by MrSwi6 transcription factor in dimorphic fungus *Metarhizium rileyi*. World J Microbiol Biotechnol 35:46. https://doi.org/10.1007/s11274-019-2619-8.
24. Song ZY, Yin YP, Jiang SS, Liu JJ, Chen H, Wang ZK. 2013. Comparative transcriptome analysis of microsclerotia development in *Nomuraea rileyi*. BMC Genomics 14:411. https://doi.org/10.1186/1471-2164-14-411.
25. Shang YF, Xiao GH, Zheng P, Cen K, Zhan S, Wang CS. 2016. Divergent and convergent evolution of fungal pathogenicity. Genome Biol Evol 8:1374–1387. https://doi.org/10.1093/gbe/evw082.
26. Hu X, Xiao GH, Zheng P, Shang YF, Su Y, Zhang XY, Liu XZ, Zhan S, St Leger RJ, Wang CS. 2014. Trajectory and genomic determinants of fungal-pathogen speciation and host adaptation. Proc Natl Acad Sci U S A 111:16796–16801. https://doi.org/10.1073/pnas.1412662111.
27. Song ZY, Yang J, Xin CY, Xing XR, Yuan Q, Yin YP, Wang ZK. 2018. A transcription factor, MrMsn2, in the dimorphic fungus *Metarhizium rileyi* is essential for dimorphism transition, aggravated pigmentation, conidiation and microsclerotia formation. Microb Biotechnol 11:1157–1169. https://doi.org/10.1111/1751-7915.13302.
28. Mah J-H, Yu J-H. 2006. Upstream and downstream regulation of asexual development in *Aspergillus fumigatus*. Eukaryot Cell 5:1585–1595. https://doi.org/10.1128/EC.00192-06.
29. Song ZY, Yin YP, Lin YL, Du F, Ren GW, Wang ZK. 2018. The bZip transcriptional factor activator protein-1 regulates *Metarhizium rileyi* morphology and mediates microsclerotia formation. Appl Microbiol Biotechnol 102:4577–4588. https://doi.org/10.1007/s00253-018-8941-5.
30. Wang JB, St Leger RJ, Wang CS. 2016. Advances in genomics of entomopathogenic fungi. Adv Genet 94:67–105. https://doi.org/10.1016/bs.adgen.2016.01.002.
31. Zhao H, Lovett B, Fang W. 2016. Genetically engineering entomopathogenic fungi. Adv Genet 94:137–163. https://doi.org/10.1016/bs.adgen.2015.11.001.
32. Chen XX, Xu C, Qian Y, Liu R, Zhang QQ, Zeng GH, Zhang X, Zhao H, Fang WG. 2016. MAPK cascade-mediated regulation of pathogenicity, conidiation and tolerance to abiotic stresses in the entomopathogenic fungus *Metarhizium robertsii*. Environ Microbiol 18:1048–1062. https://doi.org/10.1111/1462-2920.13198.
33. Lysøe E, Pasquali M, Breakspear A, Kistler HC. 2011. The transcription factor FuStuAp influences spore development, pathogenicity, and secondary metabolism in *Fusarium graminearum*. Mol Plant Microbe Interact 24:54–67. https://doi.org/10.1094/MPMI-03-10-0075.
34. Xin CY, Xing XR, Wang F, Liu JX, Ran ZN, Chen WB, Wang GX, Song ZY. 2020. MrMid2, encoding a cell wall stress sensor protein, is required for conidium production, stress tolerance, microsclerotium formation and virulence in the entomopathogenic fungus *Metarhizium rileyi*. Fungal Genet Biol 134:103278. https://doi.org/10.1016/j.fgb.2019.103278.
35. Boucias D, Liu S, Meagher R, Baniszewski J. 2016. Fungal dimorphism in the entomopathogenic fungus *Metarhizium rileyi*: detection of an *in vivo* quorum-sensing system. J Invertebr Pathol 136:100–108. https://doi.org/10.1016/j.jip.2016.03.013.
36. Saputo S, Kumar A, Krysan DJ. 2014. Efg1 directly regulates ACE2 expression to mediate cross talk between the cAMP/PKA and RAM pathways during *Candida albicans* morphogenesis. Eukaryot Cell 13:1169–1180. https://doi.org/10.1128/EC.00148-14.
37. Soyer JL, Hamiot A, Ollivier B, Balesdent MH, Rouxel T, Fudal I. 2015. The APSES transcription factor LmStuA is required for sporulation, pathogenic development and effector gene expression in *Leptosphaeria maculans*. Mol Plant Pathol 16:1000–1005. https://doi.org/10.1111/mpp.12249.
38. IpCho SVS, Tan K-C, Koh G, Gummer J, Oliver RP, Trengove RD, Solomon PS. 2010. The transcription factor StuA regulates central carbon metabolism, mycotoxin production, and effector gene expression in the wheat pathogen *Stagonospora nodorum*. Eukaryot Cell 9:1100–1108. https://doi.org/10.1128/EC.00064-10.
39. Tamura K, Stecher G, Peterson D, Filipski A, Kumar S. 2013. MEGA6: molecular evolutionary genetics analysis version 6.0. Mol Biol Evol 30:2725–2729. https://doi.org/10.1093/molbev/mst197.
40. Vandesompele J, De Preter K, Pattyn F, Poppe B, Roy NV, Paepe AD, Speleman F. 2002. Accurate normalization of real-time quantitative RT-PCR data by geometric averaging of multiple internal control genes. Genome Biol 3:research0034.1. https://doi.org/10.1186/gb-2002-3-7-research0034.
41. Östlund G, Schmitt T, Forslund K, Kostler T, Messina DN, Roopra S, Frings O, Sonnhammer EL. 2010. InParanoid 7: new algorithms and tools for eukaryotic orthology analysis. Nucleic Acids Res 38:196–203. https://doi.org/10.1093/nar/gkp931.
42. Thimm O, Bläsing O, Gibon Y, Nagel A, Meyer S, Krüger P, Selbig J, Müller LA, Rhee SY, Stitt M. 2004. MAPMAN: a user-driven tool to display genomics data sets onto diagrams of metabolic pathways and other biological processes. Plant J 37:914–939. https://doi.org/10.1111/j.1365-313x.2004.02016.x.